SUPPORTING INFORMATION

Conformational aspects of high content packing of antimicrobial peptides in polymer microgels

Shalini Singh[1], Aritreyee Datta[2], Bruno C. Borro[3], Mina Davoudi[4], Artur Schmidtchen[4,5,6], Anirban Bhunia[2,*] and Martin Malmsten[1,3,*]

[1]Department of Pharmacy, Uppsala University, SE-75232 Uppsala, Sweden

[2]Department of Biophysics, Bose Institute, P-1/12 CIT Scheme VII (M), Kolkata 700054, India

[3]Department of Pharmacy, University of Copenhagen, DK-2100 Copenhagen, Denmark

[4]Division of Dermatology and Venereology, Department of Clinical Sciences, Lund University, SE-221 84 Lund, Sweden

[5]Lee Kong Chian School of Medicine, Nanyang Technological University, 11 Mandalay Road, Singapore 308232

[6]Wound Healing Centre, Bispebjerg University Hospital, DK-2100 Copenhagen, Denmark

*To whom correspondence should be addressed:

Martin Malmsten, Tel: +45 31499203, Email: martin.malmsten@sund.ku.dk

Anirban Bhunia, Tel: +91-33-25693336, E-mail: bhunia@jcbose.ac.in

Table S1. Key properties of the peptides investigated[d].

Peptide	Sequence	M_w[a]	Z_{net}[b]	H[c]
EFK17a	E**F**KR**I**VQR**I**KD**F**LRNLV	2215	+3	-0.27
EFK17da	E(**dF**)KR(d**I**)VQR(d**I**)KD(d**F**)LRNLV	2215	+3	-0.27

a) Mw: Molecular weight (g/mol)
b) Z_{net}: Net charge at pH 7.4
c) H: Mean hydrophobicity on the Kyte–Doolittle scale (47).
d) Peptide purity >95%

Table S2. Key properties of the gels investigated.

Abbreviation	Nominal composition (wt%)			Size[a,c]	pKa	% MAA[b]	Ionization[b]
	EA	MAA	BDD				
MAA20	79.0	20.0	1.0	77	7.0	22.1±1.1	0.72
MAA60	39.0	60.0	1.0	180	6.5	63.3±1.5	0.89

a) Microgel hydrodynamic diameter (nm) determined with NTA, in 10mM Tris HCl, pH 7.4
b) Mettler Toledo titrator, 0.01M NaCl, initial pH 3.5.
c) Over the pH-range 4-11, microgel swelling is observed with increasing pH, the extent of which depends on microgel charge density, i.e., increasing with increasing content of acrylic acid residues. However, no aggregation was observed over this pH range (19).

Table S3. Summary of the structural statistics of the twenty lowest energy ensemble structures of EFK17a and EFK17da in MAA60.

Distance restraints	**EFK17a**	**EFK17da**
Intra-residue (i-j=0)	42	42
Sequential (|i-j|=1)	67	64
Medium-range (2≤|i-j|≤4)	21	10
Long-range (|i-j|≥5)	0	7
Total	129	123
Angular restraints		
ϕ	15	15
Ψ	15	15
Distance restraints from violations (≥0.4Å)		
Deviation from mean structure (Å)		
Average backbone to mean structure	0.35±0.17	0.89±0.30
Average heavy atom to mean structure	1.01±0.16	1.50±0.24
Ramachandran plot for mean structure e[a]		
% Residues in the most favourable and additionally allowed regions	100	93.3
% Residues in the generously allowed regions	0	6.7
% Residues in the disallowed regions	0	0
PDB code	5XNG	5XRX

[a]Based on Procheck NMR

Figure S1. Helical wheel projection of EFK17a with enantiomeric (dF or dI) subjections outlined. Grey and white circles represent charged/hydrophilic and uncharged/hydrophobic residues, respectively, while dF and dI represent D-amino acid substitutions made in EFK17da.

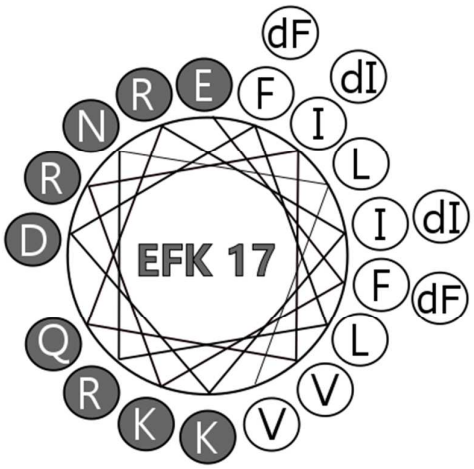

Figure S2. Representative liposome leakage experiments, show successive injections of DOPE/DOPG liposomes (t=0), EFK17a (1 μM, t=600 s) and Triton-X (0.8 mM, t=2400 s) in 10 mM Tris, pH 7.4, the latter for complete membrane rupture. For comparison, measurements with the same liposome preparation in the absence of peptide addition is shown in order to demonstrate that peptide-induced leakage induction is much larger than any background leakage.

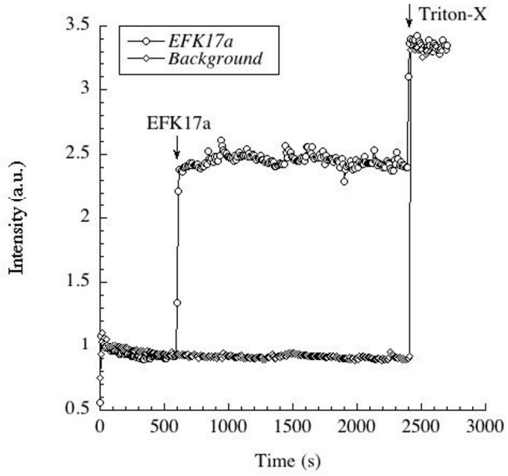

Figure S3. Thermodynamics of interaction of EFK17a and EFK17da with MAA60 and MAA20 microgels, obtained by ITC. Plots showing change in enthalpy of the microgel system per mole of peptide injection vs molar ratio (peptide:microgel) for (A) EK17a in MAA60, (B) EFK17a in MAA20, and (C) EFK17da in MAA60 microgels. The thermodynamic parameters for each of the reactions are shown in the respective plots.

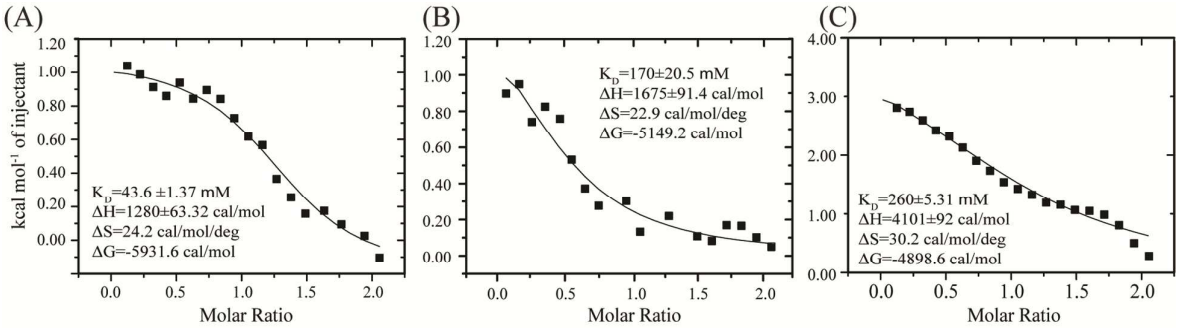

Figure S4. Mean particle size, obtained by PCS at a microgel concentration of 10 ppm and various peptide concentrations in 10 mM Tris, pH 7.4.

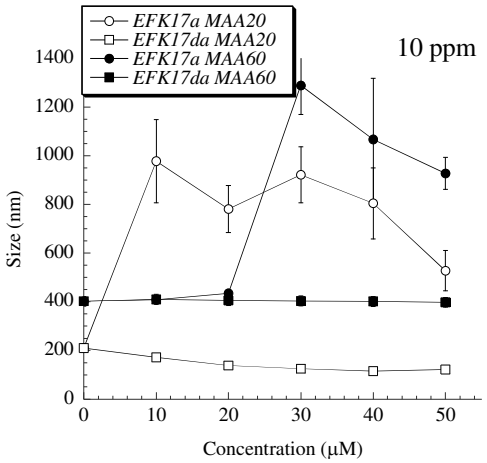

Figure S5. trNOESY spectra of EFK17a after MAA60 binding. Selected regions of the ^{1}H-^{1}H trNOESY spectra of EFK17a in MAA60, showing (A) fingerprint region presenting the backbone-amide C$^{\alpha}$H-NH resonances, (B) backbone-backbone NH-NH resonances, and (C) long-range resonances between aliphatic side-chain and aromatic ring protons.

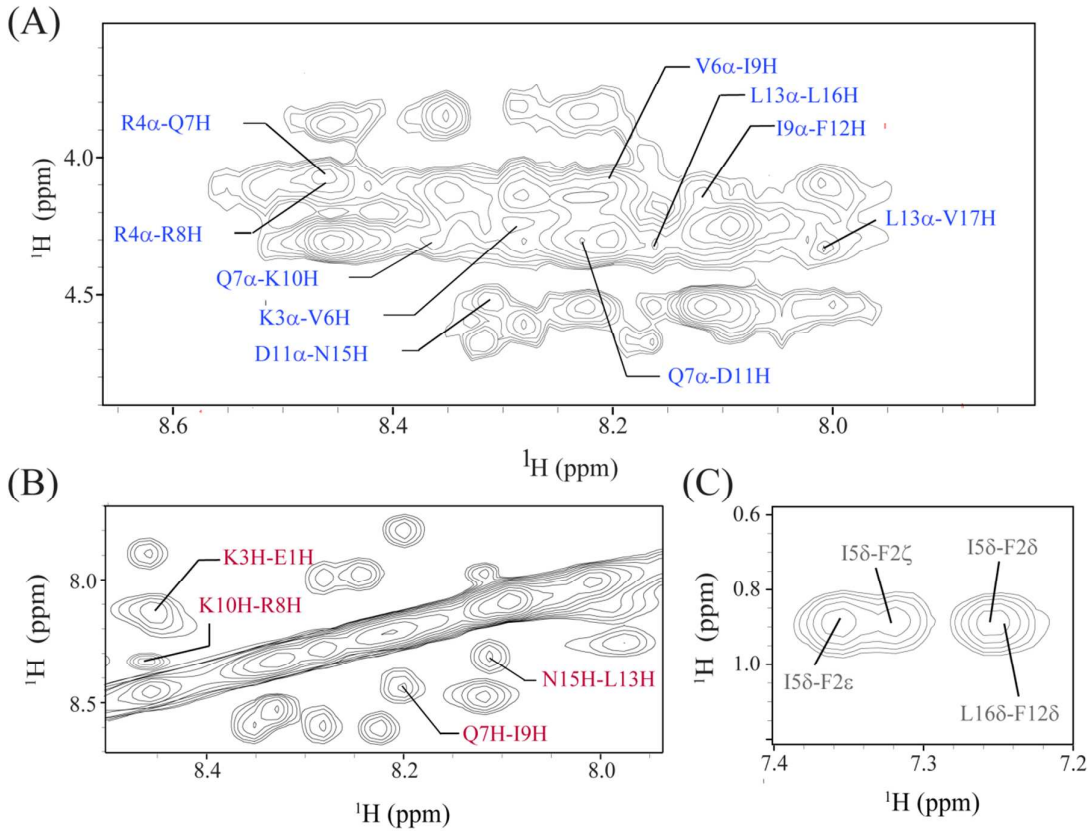

Figure S6. trNOESY spectra of EFK17da after loading into MAA60 or MAA20. (A) Overlay trNOESY spectra of EFK17da in MAA60 (blue) and MAA20 (red), showing that the two spectra are almost identical. Shown also are fingerprint region presenting (B) backbone-amide $C^{\alpha}H$-NH resonances, (C) backbone-backbone NH-NH resonances, (D) medium-range aliphatic side chain-backbone amide resonances, (E) long-range resonances between aliphatic side-chain and aromatic ring protons, and (F) long-range resonances between aromatic-aromatic ring protons.